LA-UR 93-2255

Los Alamos National Laboratory is operated by the University of California for the United States Department of Energy under contract W-7405-ENG-36

TITLE REVIEW OF THE PROCYON EXPLOSIVE PULSED POWER SYSTEM

AUTHOR(S): J. H. GOFORTH, M-6
H. OONA, M-6
A. E. GREENE, X-5
W. E. ANDERSON, MST-7
R. L. BOWERS, X-5
J. H. BROWNELL, X-5
R. E. CHRIEN, P-14
C. M. FOWLER, M-6
T. R. LINDEMUTH, X-1
C. M. LUND, X-5
S. P. MARSH, M-6
T. OLIPHANT, X-5
J. V. PARKER, P-DO
R. E. REINOVSKY, M-6
J. S. SHLACHTER, P-1
L. R. VEESER, P-14
D. T. TORRES, M-6
J. T. TABAKA, P-14
J. C. KING, M-6
D. L. WEISS, X-5
F. J. WYSOCKI, P-1
N. F. RUDERICK, UNM
P. J. TURCHI, OSU
D. H. HERRERA, M-6
B. C. ANDERSON, P-1
J. C. COCHRANE, P-1
H. F. GARCIA, P-1

SUBMITTED TO: 9TH IEEE INTERNATIONAL PULSED POWER CONFERENCE
JUNE 21-23, 1993
ALBUQUERQUE, NM

DISCLAIMER

MASTER

Los Alamos National Laboratory
Los Alamos, New Mexico 87545

REVIEW OF THE PROCYON EXPLOSIVE PULSED POWER SYSTEM

J. H. Goforth, H. Oona, A. E. Greene, D. H. Herrera, D. L. Peterson, B. G. Anderson, W. E. Anderson, J. H. Brownell, R. L. Bowers, R. E. Chrien, J. C. Cochrane, C. E. Findley, M. F. Fowler, O. F. Garcia, M. L. Hodgdon, J. C. King, I. R. Lindemuth, C. M. Lund, S. P. Marsh, T. Oliphant, J. V. Parker, R. E. Reinovsky, J. S. Shlachter, L. J. Tabaka, D. T. Torres, L. R. Veeser, D. L. Weiss and F. J. Wysocki, LANL

N. F. Roderick, UNM

P. J. Turchi, OHIO STATE UNIVERSITY

B. J Warthen, EG&G

ABSTRACT

The Procyon explosive pulsed power system is designed for powering plasma z-pinch experiments. It begins with a helical explosive-driven magnetic flux compression generator (MCG) for amplifying seed current from a capacitor bank into a storage inductor. One conductor element of the storage inductor is an explosively formed fuse (EFF) opening switch tailored to divert current to a plasma flow switch (PFS) in less than 3 μs. The PFS, in turn, delivers current to a z-pinch load. Experiments to date have concentrated on the explosive pulsed power components and PFS. This paper focuses on the results of a recent full energy MCG/EFF/PFS test. Improvements suggested by earlier experiments were incorporated into the MCG/EFF components, and the system provided current to a PFS which used a mass graded aluminum foil tailored to produce a 1/r mass distribution yan

plasma. The 1/r mass distribution is a departure from the standard practice of using a distribution of $1/r^2$, and was included as an attempt to generate a different opening posture for the PFS. In addition, improvements in foil deposition technique allowed us to use a graded foil in place of the previously used cordal wire arrays. In the test, 21.4 MA was generated in a 79 nH storage inductor providing over 18 MJ of magnetically stored energy. The EEF then diverted 16.4 MA to the PFS with a 10-90% pulse rise time of 1.6 μs. System improvements led to currents about 7% larger than in previous tests, and faster performance of the EEF. As a result, the PFS received a higher and faster current pulse than that used in preshot computations, and the overall performance was better than expected. As much as 15.5 MA was delivered to the 4-cm-radius load slot with a 10-90% rise time of 300ns. We now have a pulsed power supply that is able to drive 1 MJ implosions, and has the potential to scale beyond 2 MJ with optimized performance. For loads that can operate with lower inductance feeds and that achieve higher increases in inductance, load energies approaching 5 MJ are possible.

INTRODUCTION

In this paper, we will describe the Procyon system and its performance. We will also comment on the amount of increased performance to be obtained either by optimizing the current design or scaling the device up in size. Procyon is the name for an explosive pulsed power (EPP) system designed to drive 1 MJ plasma z-pinch experiments. We have recently completed the development of the system, which is pictured in Fig. 1. Many of the design features, goals, and preliminary data have been previously published [1,2,3,4,5] and are summarized here for completeness. A capacitor bank supplies 475 KA (0.8 MJ), which initially flows in a MK IX MCG and in a storage inductor, one wall of which is an EEF opening switch. Explosive action of the MCG amplifies current in the circuit as magnetic flux is compressed into the storage inductor (6). When peak current is achieved in the

storage inductor, the EFF is actuated producing resistance in the switch. The voltage across the switch also appears across closing switch plates, and the closing switches are actuated when the desired voltage is achieved. The opening of the EFF diverts current to a PFS (7) that isolates the implosion load from the 2 - 3 μs EFF pulse, then commutes current to the load at or near peak PFS current. The initial storage inductor current is divided inductively as flux fills each successive volume. In our most recent test, our storage inductor was 79 nH, and the power flow system associated with the PFS was 23 nH. The PFS gun was 5 nH and switched into a 2.6 nH dummy load slot. On the test, we developed 21.4 MA in the storage inductor (18.1 MJ) and diverted 16.4 MA to the PFS with a 10-90 % rise time of 1.6 μs. At this time, 13.9 MJ remain in 103 nH. The PFS for the test was designed to open in a gating action because the PFS plasma mass density varied as 1/r in the barrel where forces vary as $1/r^2$. The current pulse was larger and faster than expected, and as a result, the PFS "gated" open while only 2 - 3 cm down the 7 cm barrel. The downstream switching results are exciting, and will be described here and in another paper in the conference (8). At a probe position inside the load slot and near the upstream electrode, 15.5 MA was developed with a 10 - 90 % rise time of 500 ns. Probes in the wall of the 4 cm radius load vary and are subject to some interpretation. One dB/dt probe shows a rise to 13.9 MA with a 10-90% rise of 500 ns. On the other hand, a Faraday rotation signal shows that as much as 15.5 MA was switched with a 10 - 90% risetime of 300ns. Future efforts are directed at understanding and reproducing the switching observed.

APPARATUS

Capacitor Bank/MCG/EFF

A Procyon circuit diagram is given in Fig. 2 and a cross section of the EPP and load sections in Fig. 3. The initial energy for a Procyon test is supplied by two 3000 μF capacitor bank modules charged to ~18 KV. To shorten the energy delivery time, we connect the modules in series, effectively creating a 1500 μF, 36 KV bank. We described our two stage Marx system header earlier (9). Marx header failures during Procyon tests, however, led us to redesign the system to provide a high degree of control on the cleanliness and atmosphere around the header. Operating procedures now require the system to be flushed with dry nitrogen, then filled with SF_6 at atmospheric pressure and ambient temperature. The capacitor bank is discharged through the header into the EPP system dominated by the 7.2 μH MK-IX generator. Contributing to header failures were voltage reflections generated at the input to the 7.2 μH inductance. In tests with simulated MCG's, reflections were recorded at the Marx header that were nearly double the voltage of the two modules. To alleviate this reflection, we installed a 4 Ω resistor array at the input to the MK-IX. With these resistors in the circuit, the ringing of the header voltage is reduced as shown in Fig. 4. At that level, our new header has over a factor of two safety margin.

The MK-IX generator has been described in detail earlier (6). When the capacitor bank energy has been delivered to the MK-IX, the MK-IX explosive (HE) charge is detonated and the armature expands, closing the crowbar switch. At that time, 475 KA is flowing and the system contains 0.8 MJ magnetic energy. The explosive action systematically reduces the 7.2 μH inductance of the MK-IX, sweeping the flux into the storage inductor. The inductance, L_{sto}, in Fig. 2, is largely due to the storage inductor volume indicated in Fig. 3. The rest is resident in residual circuit volume at the MK-IX output. Fig. 5 shows a 2D hydrocode calculation of the MK-IX output region at the end of the generator operation. In the calculation, magnetic field effects are simulated by material pressures in the inert volume. Due to explosive and magnetic effects, it is difficult to predetermine the

exact value for L_{sto}, but we are able to deduce the effective value from current transfer ratios. On our recent test, a value of 79 nH is obtained for L_{sto}, which indicates that the field has increased the circuit volume substantially. In addition, the free volume at the end of the MK-IX allows the HE pressure to be relieved, and causes the armature to be retarded somewhat. The storage inductor for the Procyon device was designed carefully to avoid problems associated with high pressure magnetic field effects. Current joints are designed such that pressure brought to bear by the joint bolts equals or exceeds the magnetic pressure. In some cases material strengths are exceeded, and an effort is made to provide inertial confinement for the time scales of interest in these cases. In the storage inductor, material strengths are exceeded for approximately the last 35 μs of the pulse.

We have previously described the EFF in a variety of publications (10,11). Fig. 6 shows a 2D hydrodynamic calculation to help summarize the opening mechanism involved in these switches. Segments of a conductor that has adequate cross section to conduct a current pulse without fusing from Ohmic heating are extruded into a cross section that will fuse, producing the resistance, R_{open}, in Fig. 2. We have used EFF switches in fast applications where HE is directly in contact with the switch element (12). Subsequently, we have demonstrated that they can be slowed down by substituting inert material adjacent to the switch element, forcing the explosive to drive a larger mass (11). This is the configuration used for Procyon. Prior to our first Procyon test, we calculated that an aluminum conductor with 8 cm^2 cross sectional area would withstand the storage inductor current pulse without fusing. In a test at 20 MA with a 0.69-mm thick EFF element of 107 cm circumference, some features of the EFF voltage curve caused us to be concerned that we were approaching melt. For our recent test, we increased the thickness to 0.76 mm to assure a margin of safety. The respective EFF voltage curve is not available from the recent test, but on that test we achieved 21.4 MA storage inductor current. The 10% thickness increase does not quite compensate for the 7% increase in current, which is squared in the

action integral. Nevertheless, inordinate losses were not encountered, even at the end of the current pulse, so we are confident that we have not passed the action limit for the EFF element. However, another 10% current increase could dictate an increase in EFF thickness

We surmounted several engineering design difficulties with our EFF element by manufacturing it out of a single forging. By this method, we avoid clamping the thin material in a complicated high pressure joint, and are able to fare the thin wall into a thick end plate with a machined curve. We were initially concerned about that junction (1), but the technique has proved satisfactory.

Transfer Section

We continue to refer to the circuit in Fig. 2, but isolate the components in our transfer section in Fig. 7. The components of this triaxial section are pictured in Fig. 8. In the figure, we note a coaxial transmission section with a vacuum dielectric interface at one end of the Teflon insulation. The interface provides standoff for EFF opening switch voltage to drive current into the vacuum region, and baffles isolate the interface from radiation produced in the PFS gun. Voltage generated across the EFF as it begins to open is applied across the closing switch plates through the PFS conductor. The closing switch insulation consists of a hat that nests with the output insulator near the vacuum dielectric interface, and 1.25 mm polyester insulation. At the desired time, explosive driven jets puncture the 1.25 mm polyester and current flow begins.

The output insulator for Procyon has some special design features. We have chosen Teflon for it, as for the EFF die, because Teflon remains a good insulator at very high pressures. The insulator must withstand the system voltage for several microseconds after the the

shock wave has passed through it, and has distorted it considerably. The section at the output end of this insulator was designed carefully to prevent the explosive action from shearing it and causing a high voltage failure. In addition, we made the insulation 11-mm thick in spite of data indicating we could hold off 140 KV across 6.35-mm. As seen in Fig 7, the output insulator is nested with the closing switch hat to provide a long path between switch plates at this junction. Finally, the vacuum dielectric interface on the output insulator was incorporated in electric field calculations performed for the radiation baffle/interface section. We arranged field contours to be perpendicular to the vacuum interface, and the highest field points in the baffle region were 250 KV/cm. Further, practical experience suggests at least 5 bounces should be provided by a baffle system, and our baffles were designed accordingly. There is also information that suggests that radiation should be kept below 60 $\mu J/cm^2$ (13). By coupling attenuation measurements with RMHD calculations, we estimate that we expose the Procyon interface to 10 $\mu J/cm^2$ (14) The attenuation measurements were made with light between 300 and 600 nm in wavelength, however, but for UV light the attenuation is much greater. Therefore, the UV radiation that is responsible for the flashover is much less than the 10 $\mu J/cm^2$. We have previously described our system of six explosively actuated closing switches (2) in parallel Because we have large explosives charges in other components, we are free to use as much HE as needed to drive high quality jets As a result, we achieve good synchronization, jitter and resistance performance

PFS

The PFS for Procyon combines design features from several sources The basic concept and electrode dimensions come from experiments conducted at the Phillips Lab (7) The output vane structure is the same as used on the PFS experiments conducted at the Los Alamos Pegasus facility (15) Foil mass, mass grading, and gap length are determined by

coupling early Procyon results with a variety of calculations, and a paper dedicated to these efforts also appears in these proceedings (8). Recent tests on the Pegasus bank and our recent Procyon test employed a mass graded foil for the initial PFS conductor. Fig. 9 shows the mass distribution in the foil, and Fig. 10 shows the foil installed in the shot. The mass distribution in the aluminum is roughly $1/r^2$, and when coupled with the 3.36 μm thick mylar barrier film forms a 1/r mass distribution.

PULSED POWER CONSIDERATIONS

Figure 11 is a simple circuit that helps summarize pulsed power considerations. If a constant I_0 is flowing in the loop with constant L_{st} and R when the switch, S, is closed, then

$$I = \left(\frac{L_{pri}}{L_{pri} + L_{st}}\right) I_0 \left(1 - e^{-t/\tau}\right)$$

where $$\tau = \frac{L(L_{pri} + L_{st})}{L_{pri} L_{st}}$$

further $$\Delta I = \frac{1}{2} I_0 \left(\frac{L_{pri} L_{st}}{L_{pri} + L_{st}}\right)$$

In our tests, R and I_0 are not constants, but the equations have simple analytical forms that help us understand the important features of the pulsed power results. Also note that the flux and energy equations don't depend on time, only end points.

PULSED POWER RESULTS

Explosive Pulsed Power Results

In this section we primarily show the results form our most recent test, with comparison to earlier tests when useful. We have three tests which will be referred to as T1, T2, and T3

respectively for ease of identification. T1 was our earliest test, and was conducted at ~10% lower than nominal current. T2 was our first attempt at a nominal energy experiment and it experienced a transmission line failure because the closing switches were not adequately synchronized with the EFF. Important data came out of T2, however, (2,3) and it was this test that provided most of the insight for subsequent design improvements. T3 is our most recent test. It is another nominal energy test, and system improvements provided an additional 7% in storage inductor current over T2. Fig. 12 shows I_{sto} plotted for all three tests. The spike at the peak of these curves is due to flux compression in the EFF, and we will refer to the current just prior to the spike as peak storage inductor current. On T3 at that time, with the derived L_{sto} of 79 nH, we have 18.1 MJ available in the inductive store. Unfortunately, ground loops present on the test affected high sensitivity signals, and there is uncertainty in our initial current. The curve in Fig. 12 derives from Faraday rotation data (16) which is not affected by ground loops. Redundant sensors are available to generate the T3 curve, but signals were off scale during early times. We have shifted the T3 curve up by 0.511 MA to account for initial current and early MCG multiplication. This shift makes the T2 and T3 curves coincident at 200μs, which is a reasonable approach since both tests were fired with 18.4 KV on each bank module. The T3 curve demonstrates better generator gain and suggests that system improvements helped. Calculations indicate that the increased EFF element thickness accounts for a small amount of improvement. Additionally, the current joint between the MCG and storage inductor was observed to be glowing brightly at the end of both T1 and T2. Prior to T3, this joint was redesigned, and framing camera data revealed no glow at the joint on T3.

Fig. 13 shows the current delivered to the PFS on T3. This is a typical Faraday rotation probe signal, and is one of three located in separate places between the closing switches and the initial PFS conductor position. To interpret these signals, individual phases of the signals were analyzed, taking advantage of quadrature information, in some cases, and in others, polarity reversal information from a Rogowski coil near the closing switches. There

are minor differences between signals, but agreement among them allows us to say with confidence that 16.4 MA was delivered to the PFS. The 10-90% risetime of this curve is 1.56 μs. Preshot calculations used 20MA peak for I_{sto}, and a combination of early and late EFF resistance profiles from T2 and T1 respectively. These were the best empirical data available prior to T3. These calculations predicted a rise to 15 MA with a 10-90% time of 2.1μs. The higher and faster current rise that occurred had interesting effects on the PFS switch performance as we will discuss later. With 16.4 MA flowing and the PFS plasma advanced ~2-cm downstream, we have 79 nH in L_{sto}, and ~24 nH in the load circuit. At that time we have 13.9 MJ stored energy, and ~1.7 MJ inside the vacuum.

Fig. 14 shows $d(I_{sto})/dt$, a signal that is very important to the understanding of T3. We have marked several specific points on Fig. 14. The sudden increase in dI/dt seen at A indicates the EFF element has begun to move into the forming die. The noise on the signal at B conveniently denotes closing of the detonator switches. C marks the peak negative swing in $d(I_{sto})/dt$ while the current is being transferred into the PFS. D and E reflect final stage vacuum switching results. D is the time at which flux suddenly begins to fill the remaining load volume, and E is the time of peak transfer.

Fig. 15 shows $d(I_{PFS})/dt$ as determined from Faraday and Rogowski coil data. Initial and final segments of the signal are from Rogowski coil signals. The Rogowski coil signal gives a better initial step, but it went off scale because of the ground loop. The peak of the signal is from Faraday data. By performing a crude smoothing on the curve, we estimate that the peak of this signal is ~ 11.5 MA/μs. By joining these two curves we have learned that the nominal Rogowski coil calibration is incorrect. The integral of the smooth curve in Fig. 15 agrees well with Faraday rotation data. A factor of three adjustment of the calibration was necessary to accomplish this, however. We are searching for sources for this error, but

believe that the interpretation shown here is correct. There is further corroboration in our analysis of R_{EFF} that will be presented later.

Using the signals in Figs. 14 and 15 we can make a self consistency argument to help determine the amount of inductance reduced in L_{sto} and added to L_{PFS} by the EFF flux compression. Since peak $d(I_{PFS})/dt \approx 11.5$ MA/μs at the same time as peak negative $d(I_{sto})/dt \approx 4.3$ MA/μs, and since we know that whatever inductance is taken out of the store is put into the PFS, we can determine that 4 nH is the difference, and that $(L_{sto})(d(I_{sto})/dt)-(L_{PFS})(d(I_{PFS})/dt)\approx 320$ KV, the voltage across the EFF at peak transfer rate. At E $d(I_{sto})/dt \approx -2.4$ MA/μs. By this time we may approximate that the entire circuit downstream from the switch plasma is a single loop. (R_{EFF} is large). There is 12.79 nH upstream from the vacuum dielectric interface, and with the PFS plasma effectively 2.5-cm down the gun barrel, we have 11.11.5 nH between the PFS plasma and the vacuum dielectric interface. At peak flux transfer into the load, E, the voltage at the vacuum dielectric interface is 220 KV. The voltage that would cause the EFF to restrike at time E is 190 KV

The resistance of the EFF is determined in two ways. After switch closure, it is approximated by

$$R_{EFF} \approx \frac{V_{vac} - L_{vac}\, dI_{vac}/dt}{I_{vac}}$$

There is a dI/dt term not accounted for in this equation that is significant in early time, but very difficult to estimate. We also normally measure voltage across the closing switch plates, which allows a precise R_{EFF} determination before switch closure. This signal from E3 was unusable, however. To obtain a complete R_{EFF} curve, we have combined pre closure results from E2 with post closure results from E3 as shown in Fig. 16. The E2 and E3 curves should be very similar, and since switch closure never occurred on E2, pre

closure data extend well beyond what would be available from T3. After switch closure, small values for R_{EFF} are not very accurate, so the use of the T2 curve is not a bad compromise. To combine the two curves we established the value for R_{EFF} when the closing switch actuated. This is done by measuring the initial step on the $d(I_{PFS})/dt$ curve, then calculating the related voltage and dividing by I_{STO}. We then moved the T2 curve to agree at that time, and joined the curves. Our initial attempt did not procuce a good fit. After determining that our Rogowski coil signal was not properly calibrated, as noted in the discussion of $d(I_{PFS})/dt$, we made the same correction for the initial R_{EFF} value and obtained the fit shown in Fig. 16. The self consistency between these signals allows us to have confidence in this interpretation, even though we are not sure of the source of the error

Vacuum Switching Results

The Procyon system combines an MCG and two opening switch stages. We have described the EPP system that delivered 16.4 MA to a PFS with 10 - 90% risetime of 1.6 μs. The final pulse compression is provided by a PFS Data on PFS operation is available from two sources The Phillips Laboratory Shiva program performed the pioneering work on the concept, and more recently we have been collecting data on the Los Alamos Pegasus facility(15) As part of our program, 2D RMHD calculations are compared to the Shiva and Pegasus experiments With successive iterations, we have gained confidence in our ability to match experiment and calculation However, the predictive capability that gives good agreement with Pegasus experimental results also predicts that following the conventional approach for PFS design will not lead to good PFS performance on the Procyon system In particular, wall effects that are problematic for Pegasus appear overwhelming for Procyon Furthermore, the tricks that solve the problems for Pegasus do not help Procyon Conventional PFS design utilizes a two material concept to generate the

gun plasma. A low mass conducting material connects the two electrodes at the breach of the gun. This rapidly turns into plasma as current begins to flow. The second component is a plastic film that stops thermal plasma from flowing down the gun barrel until bulk plasma motion reaches that position. The sum of the masses of the two materials varies as $1/r^2$ across the plasma channel so that the mass will be accelerated uniformly by the $1/r^2$ magnetic force. In most work to date, the conductor mass distribution was generated by a cordal wire array, which could be varied by the number and size of wires and the cord angle. The plastic film is a constant density film. Recent developments have allowed the use of mass graded foil in place of wire arrays and Pegasus experiments have used a graded foil that varies as $1/r^{2.7}$, which combined with the barrier film yields a $1/r^2$ distribution. After a variety of calculations, a new scheme was proposed for Procyon. In this scheme, a $1/r^2$ graded foil is combined with a barrier film to produce a total mass distribution that varies as $1/r$. For 200 mg total plasma mass, we use 130 mg of aluminum in the graded foil and 70 mg in the polyester barrier film. Preliminary design calculations showed that this mass distribution, with higher pressure near the inner wall of the coaxial gun, allowed the plasma near the inner electrode to get progressively further ahead of the plasma at the outer electrode. Eventually a mass thinned region occurs and flux rapidly flows through it. Using data from early Procyon tests, the mass and gun length were chosen so that the rupture would occur as the plasma was adjacent on the implosion load slot. A plasma trap in the inner electrode wall, as used on Pegasus (16), seemed to also help in the calculations, but for preliminary tests we decided not to include this feature. T3 produced a higher and faster current pulse than predicted from earlier data. The resulting vacuum switching was very good, and in this section we present a summary of the results and our best interpretation as of this writing. A more detailed description is also included in this conference (8). An array of 20 dB/dt probes was installed in T3 downstream from the barrier film. In addition, there were two Faraday rotation probes and an electron density interferometer. The large array was in an attempt on track the gating action of the gun plasma, and track the current

switched into the load slot. Fig. 17 shows diagnostics locations. The ground loop on the test caused dB/dt data to be very noisy, and not provide as much quantitative information as we would like. A consistent trend is evident, however. The tendencies indicated in preliminary calculations were born out by T3, but the increased drive current provided a different over-all switching effect. The mass-thinned region occurred after the plasma had moved only 2-3 cm down the 7-cm barrel, and flux flooded past the PFS and filled the remaining volume in only a few hundred nanoseconds. In addition, current rose to approximately full values along the inner electrode, but not along the outer electrode. On those signals current appears to rise to some level, dips, then rises again slowly. One of the most exciting results was provided by a probe just inside the load slot along the upstream glide plane. This probe was positioned to discriminate between current flowing in a wall plasma that shorts out the load slot and current that is diverted, as desired, to the load. Subject to some interpretation, the probe shows that current rose to 15.5 with a 10- 90% risetime of 500 ns, demonstrating that wall plasma did not short out the load. The probes at the bottom of the load slot gave varying results, some of which require some interpretation. The most pessimistic interpretation comes from a dB/dt probe that shows current rising to 13.9 MA with a 10-90% risetime of 500 ns at the upstream side of the slot. The same probe went abruptly to 12-13 MA (10-90% rise of ~ 350 ns). The most optimistic signal comes from a Faraday probe in the middle of the load slot that shows current rising to as much as 15.5 MA with a 10-90% risetime of 300 ns. Figs. 18 and 19 shows selected probe data. The electron density interferometer data corroborates the dB/dt data. The data show plasma arriving at the laser path coincident with the magnetic flux as measured by the dB/dt probes. The interferometer data gave one full fringe of rotation in the next 80 ns, at which time the signal amplitude dropped to zero, probably due to hole-closure. At this time, the path averaged electron density had risen to $1.8 \times 10^{17}/cm^3$

Calculations with the actual T3 PFS drive current are currently underway to gain a better understanding of the test results. Initial calculations of this type provided several qualitatively similar features, but failed to predict the over all result. Subsequent calculations were conducted with varying initial plasma conditions, and one set with generally good agreement has now been performed. Figure 20 shows the calculations at three time steps of interest. In these calculations the mass thinned region releases the flux to the rest of the volume well within the barrel. Plasma then folds over and shunts current away from the outer electrode. Load slot calculations remain to be done, and these should help with further interpretation of our load slot data

CONCLUSIONS

A wealth of information is available from T3 and we have not yet fully digested the results We continue to explore the relevant physics for a better understanding of the vacuum switching. However, the primary difficulty encountered in calculations and earlier tests is the flooding of the load slot with plasma of sufficient density to retard the magnetic field flowing to the load and add significant (or overwhelming) mass to the implosion. The attempt to circumvent these effects by altering the mass distribution in the gun appears to be successful and we are greatly encouraged. Our next efforts will be to explore reproducibility and our degree of control

The results provided by the EPP system are also pleasing. Making simple figure of merit calculations (i e implosion Energy $\propto$ 1/2 Al. Ipfs^2), with the usual assumption of Al $\propto$ 10 nH, we claim that we have demonstrated the ability to drive 1.5 MJ implosions with a working PFS There are several sources for improvement as we seek to optimize the Procyon system, or scale it to higher energies Optimization possibilities include reducing

the thickness of our Teflon output insulator and reducing the over all inductance of our radiation baffles. We estimate that as much as 9 nH could be eliminated and still have a working system. This by itself would allow us to reach the 1.4 MJ level by the standards use above. In addition, if the vacuum switching observed is sufficiently reproducible, then we can reduce the length of the PFS gun, and can further add to the implosion drive current. On T3, the total load inductance (from EFF to 4-cm radius load slot) was 30.6 nH. With 79 nH storage inductance and 21.4 MA flowing, 15.4 MA should be transferred. This is in quite good agreement with the interpretation of our load slot Faraday sensor. With the optimized transmission line suggested above, we could achieve 1.5 MJ. Finally, with no significant system changes we could take advantage of the full 20 KV bank voltage available to us. This should boost peak storage inductor current to 23.3 MA, and using all the improvements suggested above, we could transfer 18.9 MA, or have 1.8 MJ available. Beyond these limits, the size of the EFF would probably have to increase. Another 10% current capacity is available, by increasing EFF diameter, without pushing our explosive manufacturing capability. This would require a slightly revised MCG, but with the extra 10 % we could transfer over 20 MA, and have over 2 MJ to work with.

These estimates are based on requirements for driving high radiation imploding loads. That is, these loads require radiation baffles and will probably only achieve a ΔL_f of ~10 nH. For systems that can operate with lower inductance feed sections and achieve higher values for ΔL_f, much larger energies are available. For instance, to drive a non-radiating liner 5-cm in height, our transmission line inductance could drop to ~10 nH, and ΔL_f could easily be 25 nH. Then (79/89)(21.4 MA) = 19 MA should be available to drive the implosion, and 1/2 A L_f^2 = 4.5 MJ.

References

1. J. H. Goforth, R. S. Caird, C. M. Fowler, A. E. Greene, M. L. Hodgdon, I. R. Lindemuth, S. P. Marsh, H. Oona, and R. E. Reinovsky, "Design of an Explosive Pulsed Power System for Driving 16-MA Plasma Flow Switch Experiments," in *Proceedings of the Megagauss Fields and Pulsed Power Sustems*, 1989, V. M. Titov and G. A. Shvetsov, Eds. (Nova Science Publishers, New York, 1990), pp. 651-658.

2. J. H. Goforth, H. Oona, J. H. Brownell, A. E. Greene, H. W. Kruse, I. R. Lindemuth, S. P. Marsh, J. V. Parker, R. E. Reinovsky, D. G. Rickel, and P. J. Turchi, "Procyon Experiments Utilizing Explosively-Formed Fuse Opening Switches," in *Proceedings of the 8th IEEE Pulsed Power Conference*, 1991, R. White and K. Prestwich, Eds., (1991), pp. 273-276.

3) J. H. Goforth, H. Oona, C. M. Fowler, D. H. Herrera, J. C. King, and P. J. Turchi, "Explosively Driven Opening Switch for the 20-Meganipere Procyon Experiments," *in the Proceedings of the Sixth International Conference on the Generation of Megagauss Magnet ic Fields*, 1992, to be published.

4. A. F. Greene, R. L. Bowers, J. H. Brownell, J. H. Goforth, H. Oona, D. L. Peterson, and D. L. Weiss, "Computational Modeling of the Trailmaster Procyon System," *Op. Cit.* Ref. 2, pp. 641-644.

5 I. R Lindemuth, R. E. Reinovsky, and J. H. Goforth, "Exploding Metalic Foil Fuse Modeling At Los Alamos," Op. Cit. Ref 1, pp. 269-274.

6 C. M Fowler and R. S. Caird, "The MK-IX Generator," in Proceedings of the 7th IEEE Pulsed Power Conference, 1989, B. H. Bernstein nnd J. P Shannon, Eds., (1989), pp 475-478

7) W. L. Baker, J. D Beason, J. H. Degnan, K. E. Hackett, D. J Hull, J. L. Holmes, D. W Price, J. D Graham, E. A. Lopez, G Bird, C. B. Bayer, S. K Coffey, J. F Davis III, S. W Seiler, P. J Turchi, J. S Buff, M. H Frese, R. E Peterkin, and N. F Roderick, "Plasma Flow Switch Driven Implosions," *Op. cit.* Ref 1, pp 615-622

8) R. L. Bowers, J. H Brownell, A. E. Greene, K. D McLenithan, D. L. Peterson, N. F Roderick, and P. J Turchi, "Computer Modeling of Plasma Flow Switches High Current Switching on Procyon," this conference

9) J. H Goforth, R. S Caird, C. M Fowler, A. F Greene, H. W Kruse, I. R Lindemuth, H. Oona, and R. E Reinovsky, "Performance of the Laguna Pulsed Power System," in Proceedings of the 6th IEEE Pulsed Power Conference, 1987, P. J Turchi and B. H Bernstein, eds., pp 445-448

10) J. H Goforth and S. P Marsh, "Explosively Formed Fuse Opening Switches for Use in Flux Compression Generator Circuits," in *Proceedings of the Megagauss Fields and Pulsed Power Systems* 1989, V. M Titov and G. A Shvetsov, Eds. (Nova Science Publishers, New York, 1990), pp. 515-526

11) J. H. Goforth, I. R. Lindemuth, S. P. Marsh, and R. E. Reinovsky, "Experiments with Explosively Formed Fuse Opening Switches in Higher Efficiency Circuits," in Proceedings of the Seventh IEEE Pulsed Power Conference, 1989, B. H. Bernstein and J. P. Shannon, eds., pp. 479-482.

12) J. H. Goforth, H. Oona, R. R. Bartsch, J. H. Brownell, R. S. Caird, J. C. Cochrane, D. J. Erickson, C. M. Fowler, A. E. Greene, M. L. Hodgdon, H. W. Kruse, I. R. Lindemuth, J. V. Parker, R. E. Reinovsky, and R. J. Trainor, "Explosive Pulsed Power System for Driving Laguna Foil-Initiated Plasma Implosion Experiments," *Op. Cit.* Ref. 1

13) H. Oona, B. G. Anderson, J. C. Cochrane, C. E. Findley, J. H. Goforth, A. E. Greene, H. W. Kruse, J. V. Parker, and D. G. Rickel, "Plasma and Electrical Diagnostics for Procyon Experiments," *Op. Cit.* Ref. 2, pp. 633-636.

14) J. H. Goforth, W. E. Anderson, R. R. Bartsch, J. F. Benage, R. L. Bowers J. H. Brownell, J. C. Cochrane, C. A. Fenstemacher, L. R. Foreman, P.R. Forman, C. M. Fowler, A. E. Greene, R. F. Gribble, H. W. Kruse, J. S. Ladish, C. M. Lund, S. P. Marsh, K.D. Melenithan, T. Oliphant, H. Oona, J. V. Parker, D. L. Peterson, R. E. Reinovsky, D. G. Rickel, J. S. Shlachter, D. L. Weiss, F. Wysocki, N. F. Roderick, and P. J. Turchi, "The Los Alamos Trailmaster Program: Status and Plans," Op. Cit. Ref. 3.

15) J. C. Cochrane, R. R. Bartsch, J. F. Benage, P.R. Forman, R. F. Gribble, M. Y. P. Hockaday, J. S. Ladish, H. Oona, B. Papatheolinis, J. V. Parker, J. S. Shlachter, and F. J. Wysocki, "Plasma Flow Switch Experiments of Pegasus II," this conference.

16) F. J. Wysocki, R. R. Bartsch, R. L. Bowers, J. C. Cochrane, A. E. Greene, J. S. Ladish, P.H.Y. Lee, J. V. Parker, D. L. Peterson, N. F. Roderick, and P. J. Turchi, J. F. Benage, R. F. Gribble, J. S. Shlachter, and D. W. Scudder, "Design and Characterization of the Pegasus I Plasma Flow Switch," *Op. Cit.* Ref. 3

Fig. 1 Procyon assembly ready to test in April 1993.

Fig. 2. Procyon circuit. C_1 and C_2 are two 3000μF capacitor banks arranged in series with a special header. L_W and R_W are cable and bank inductance and resistance. The 4Ω resistor prevents large voltage reflections at the input to the MK-IX MCG, L_G, when the switches S_1 and S_2 close. MK-IX explosives close the crowbar switch, S_3, as the MCG begins to operate. L_{STO} is the storage inductance into which the MK-IX drives the magnetic flux in the system. R_{OPEN} is the resistance of the OPF opening switch. When S_4 closes, current flows to the PFS. L_{TL} and L_{BARR} are associated with transmission line and radiation baffles in the output section and L_{PFS} is the increasing inductance of the PFS. A 2.6 nH load is shown.

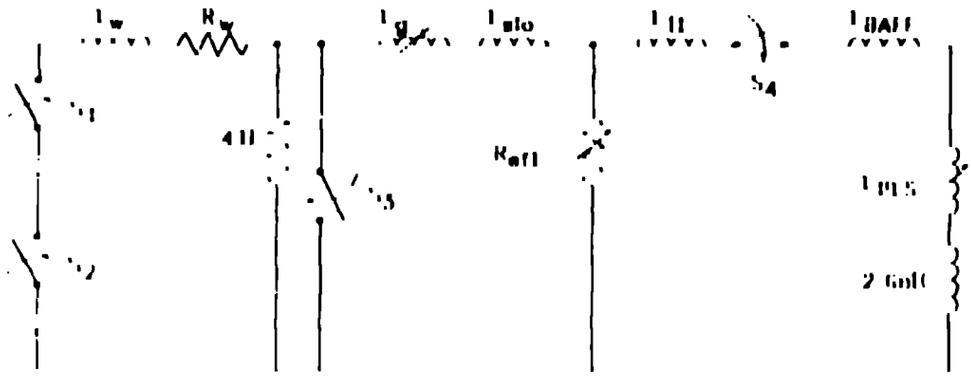

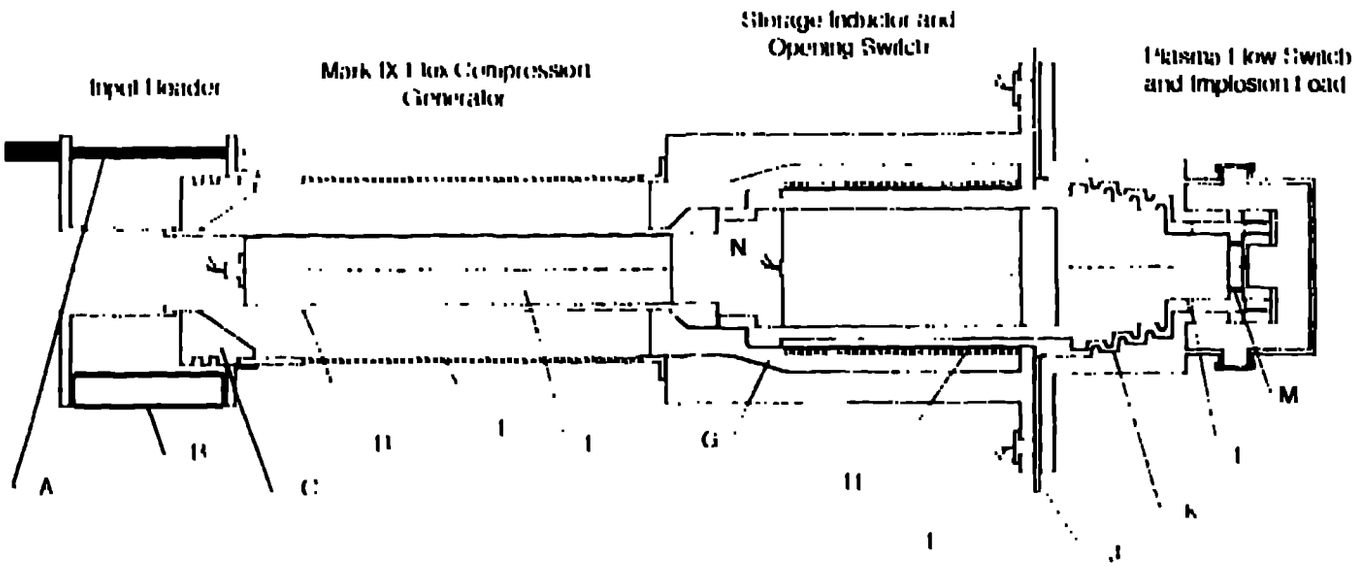

Fig. 3. Cross section of the Procyon explosive pulsed power system. The three major segments are noted, as well as the input header and the components: A- Typical input cable; B- Typical resistor in a 4Ω array, C- Input insulator, D- MK-IX armature; E- MK-IX stator, F- MK-IX HE, G-Teflon EFF forming die and storage inductor insulator; H-EFF switch element, I-Detonator actuated closing switches, J- closing switch insulation; K-radiation baffles, L- PFS conductor and barrier film; M- 4-cm radius load slot; and N- free volume housing the firing unit for EFF detonators.

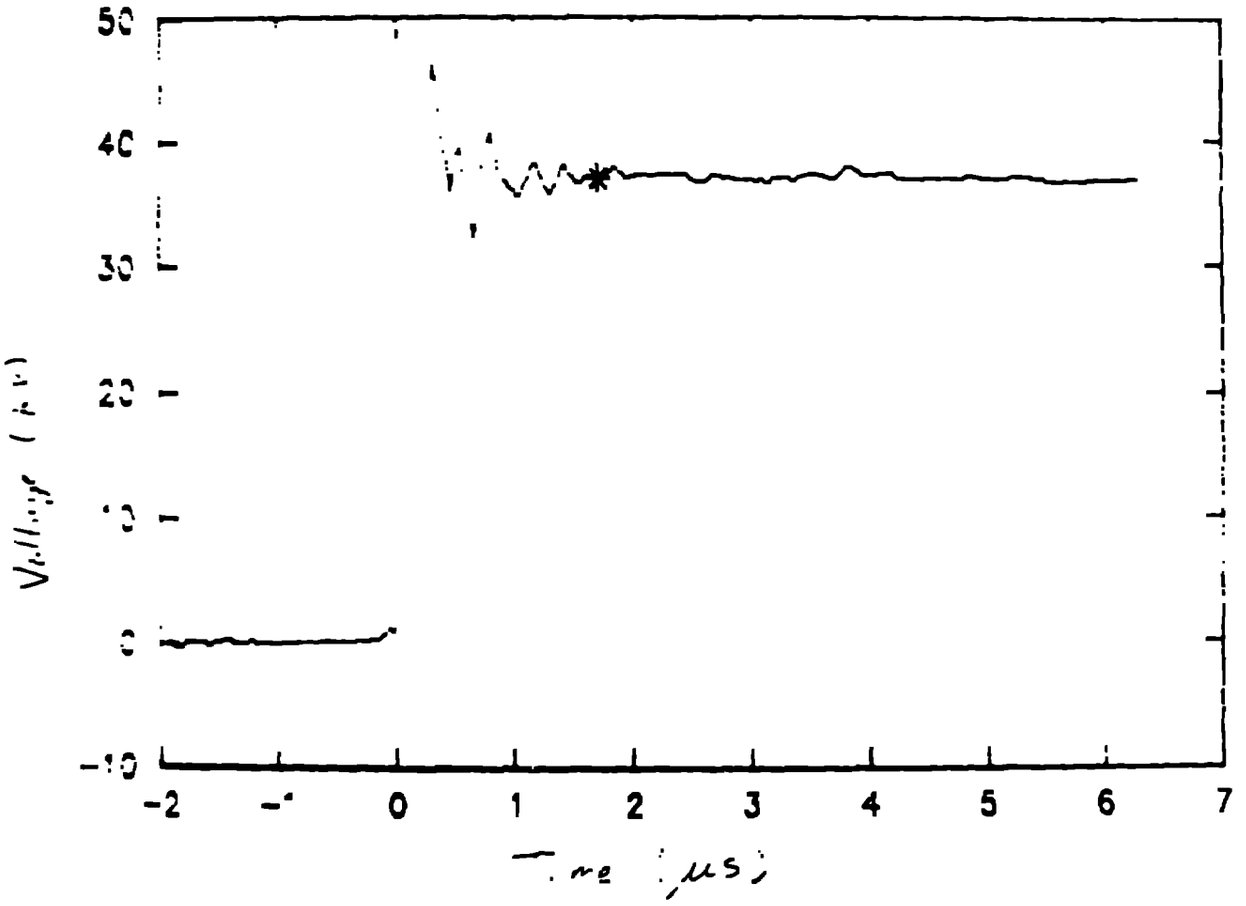

Fig 4 Voltage measured on a recent Procyon test at the Marx header.

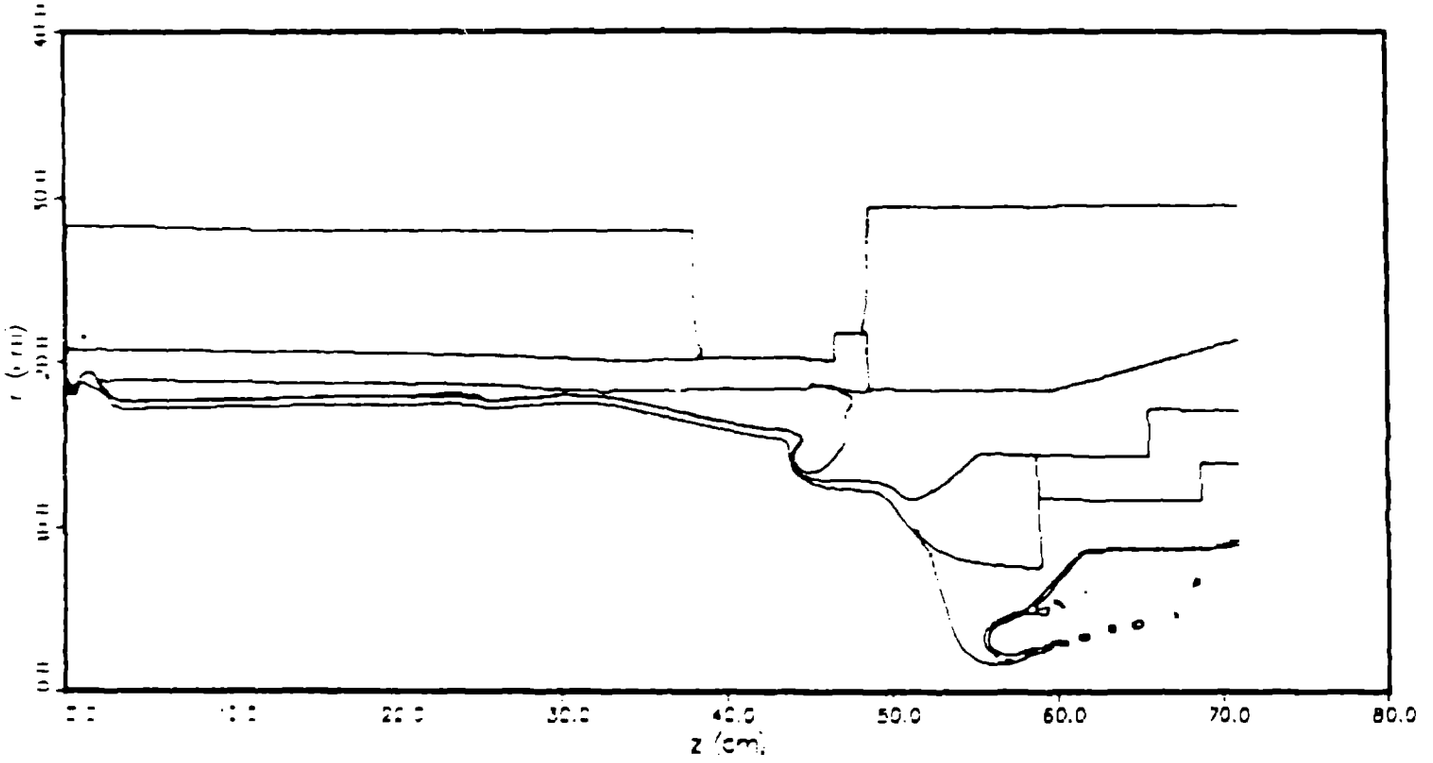

Fig 5 2-D hydrodynamic calculation of late time MK-IX output configuration.

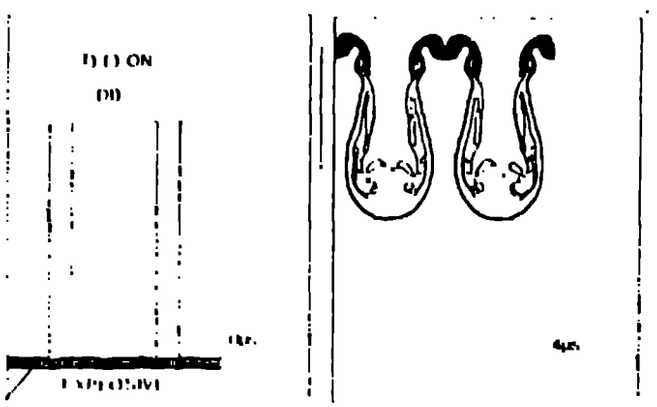

Fig. 6 Synopsis of EEF performance. The aluminum shown at t 0 is extruded into the shape shown at t 4 μs by the explosive. The thin sections of the EEF will fuse from Ohmic heating at an appropriate current density For Procyon experiments, the EEF switch element is an aluminum conductor 0.76-mm thick. The element is actuated while carrying 0.2 MA/cm of conductor width and dissipates 4.2 MJ of circuit energy

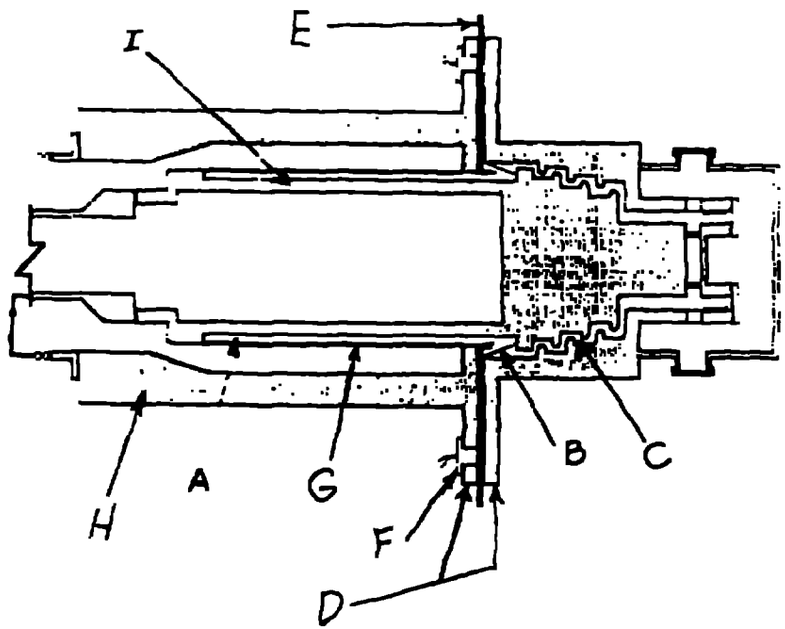

Fig 7 Transfer section A- Coaxial output transmission line insulator (Teflon); B-Vacuum dielectric interface, C- Radiation baffles to protect vacuum dielectric interface; D- closing switch plates. E- nested insulator hat and 1.25-mm polyester insulation; F- detonator actuated closing switch (array of six in parallel); G- EFF switch element; H- Outer conductor of storage inductor; I- Output conductor.

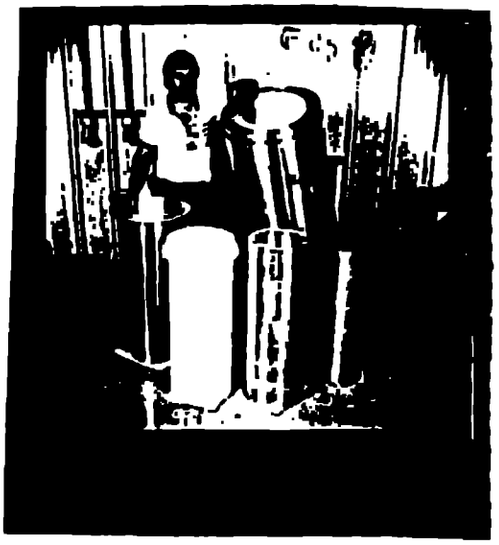

Fig. 8 Cylindrical components of the Procyon transfer section. From left to right on the floor: A- EtF switch element; B- output insulator; C- output conductor; D- air lens for the IIE system. Mounted on the stand is the outer wall of the storage inductor with the EtF die and storage inductor insulator installed.

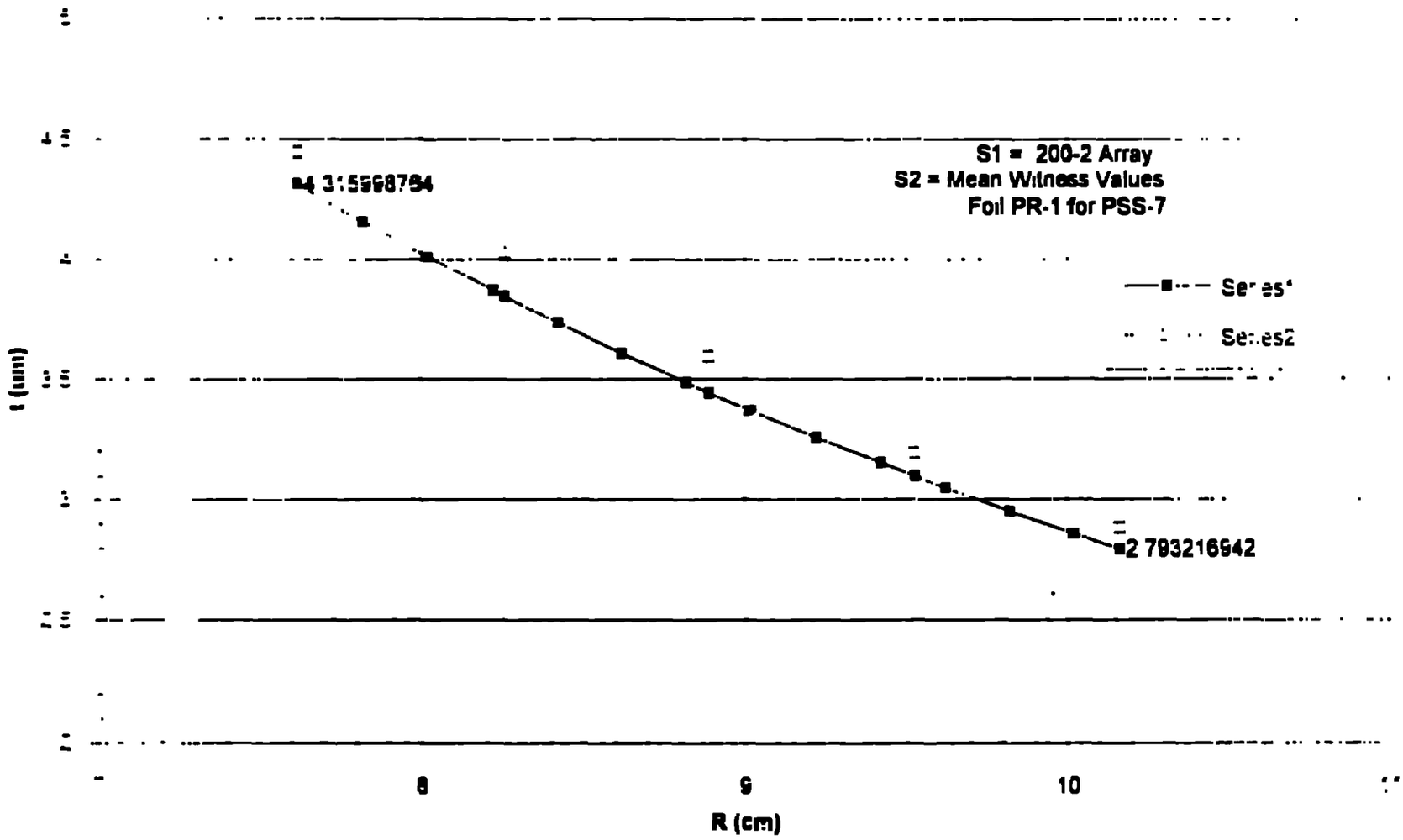

Fig. 9 Thickness profile for the Procyon mass graded foil. This distribution varies as $1/r^2$. Coupled to the barrier film, the mass distribution varies as $1/r$.

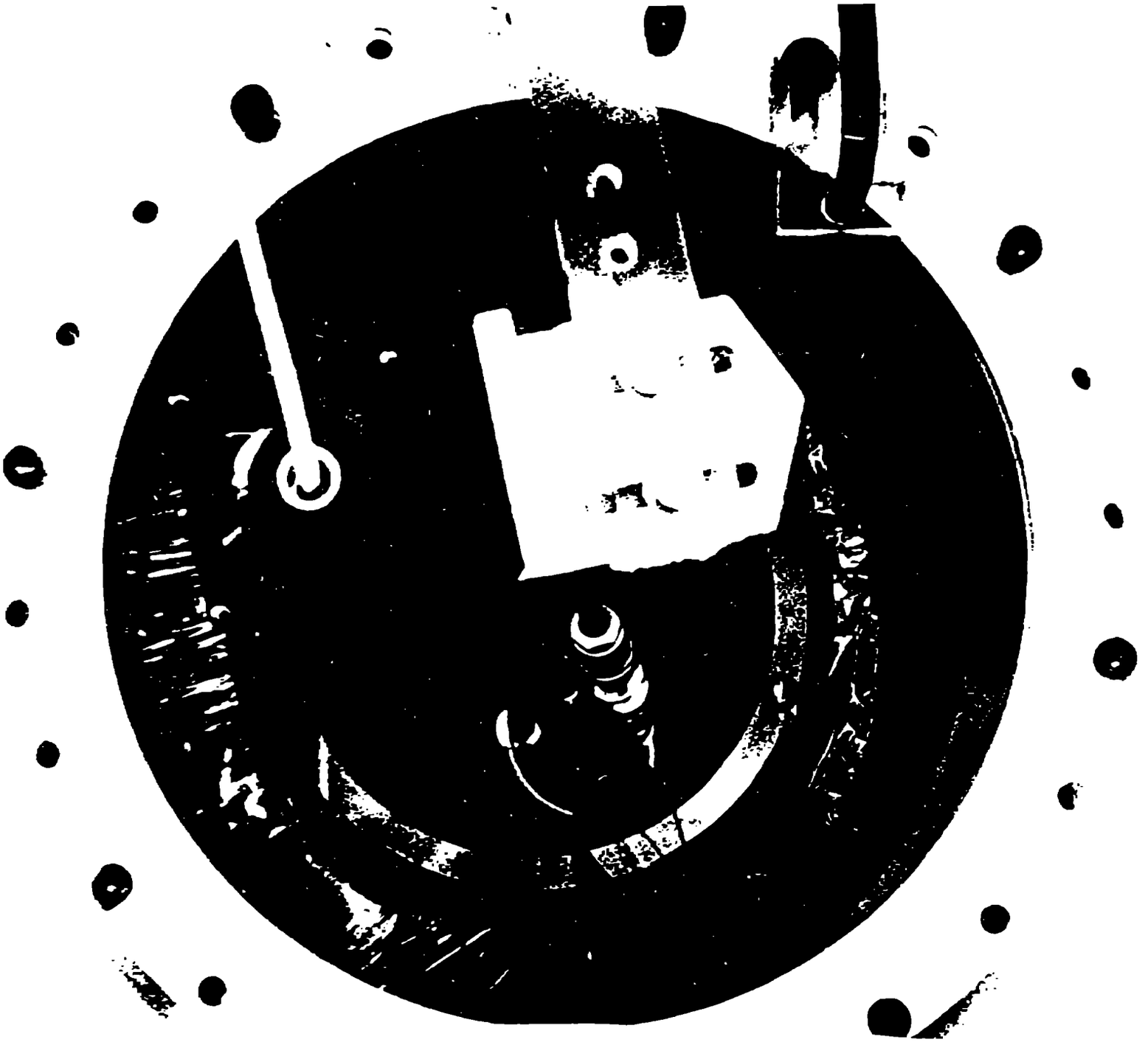

Fig 10 End view of the Procyon vacuum chamber showing the mass graded foil as installed

Fig. 11 Circuit for simple analytical current transfer analysis.

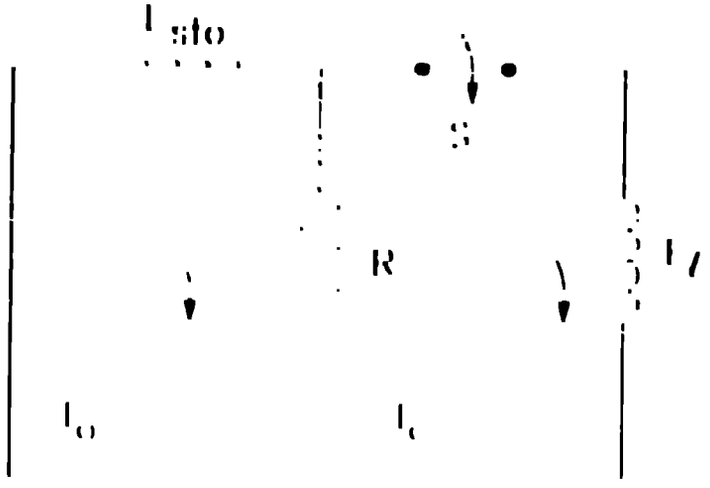

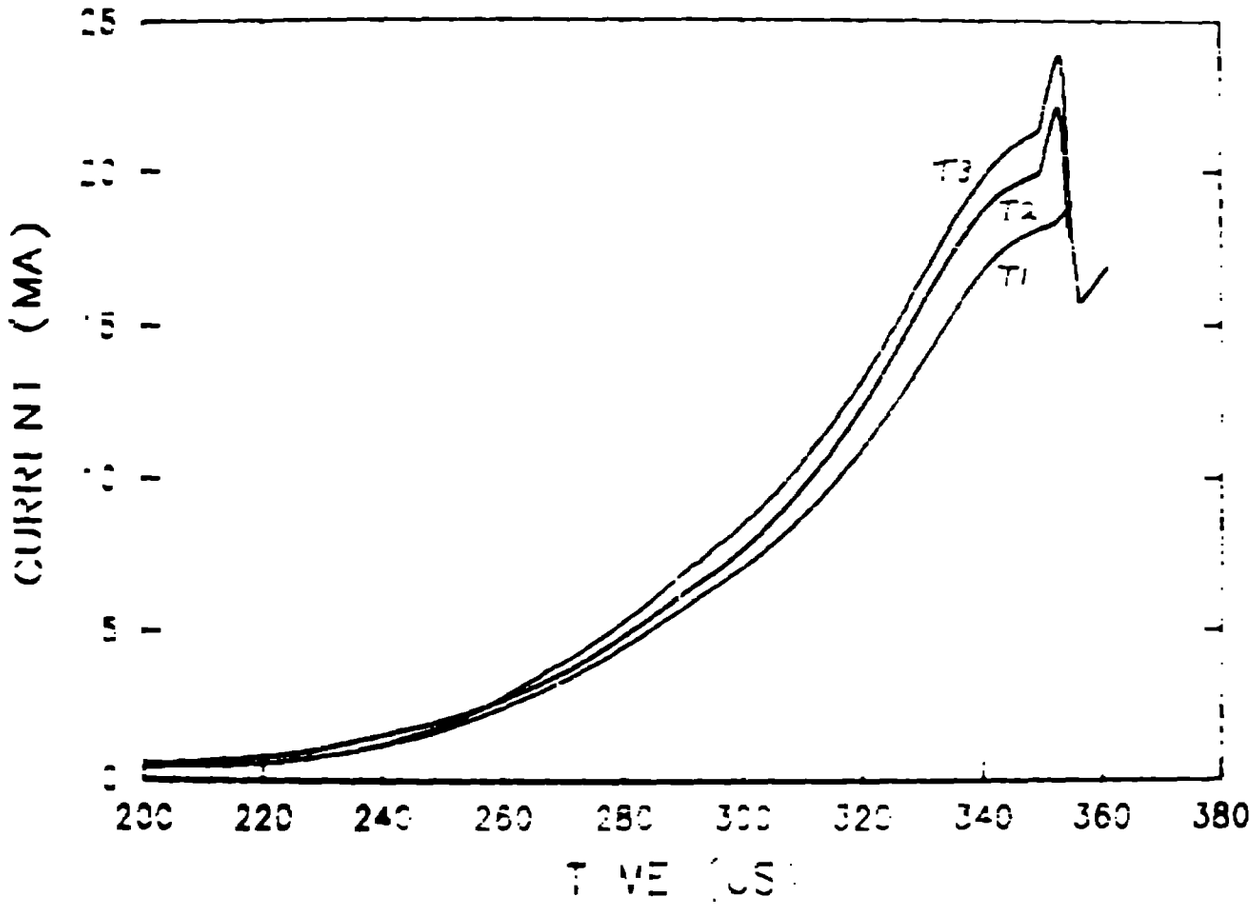

Fig. 12 Storage inductor currents from tests T1, T2, and T3. This time window includes most of the MCG amplification and all transfer segments.

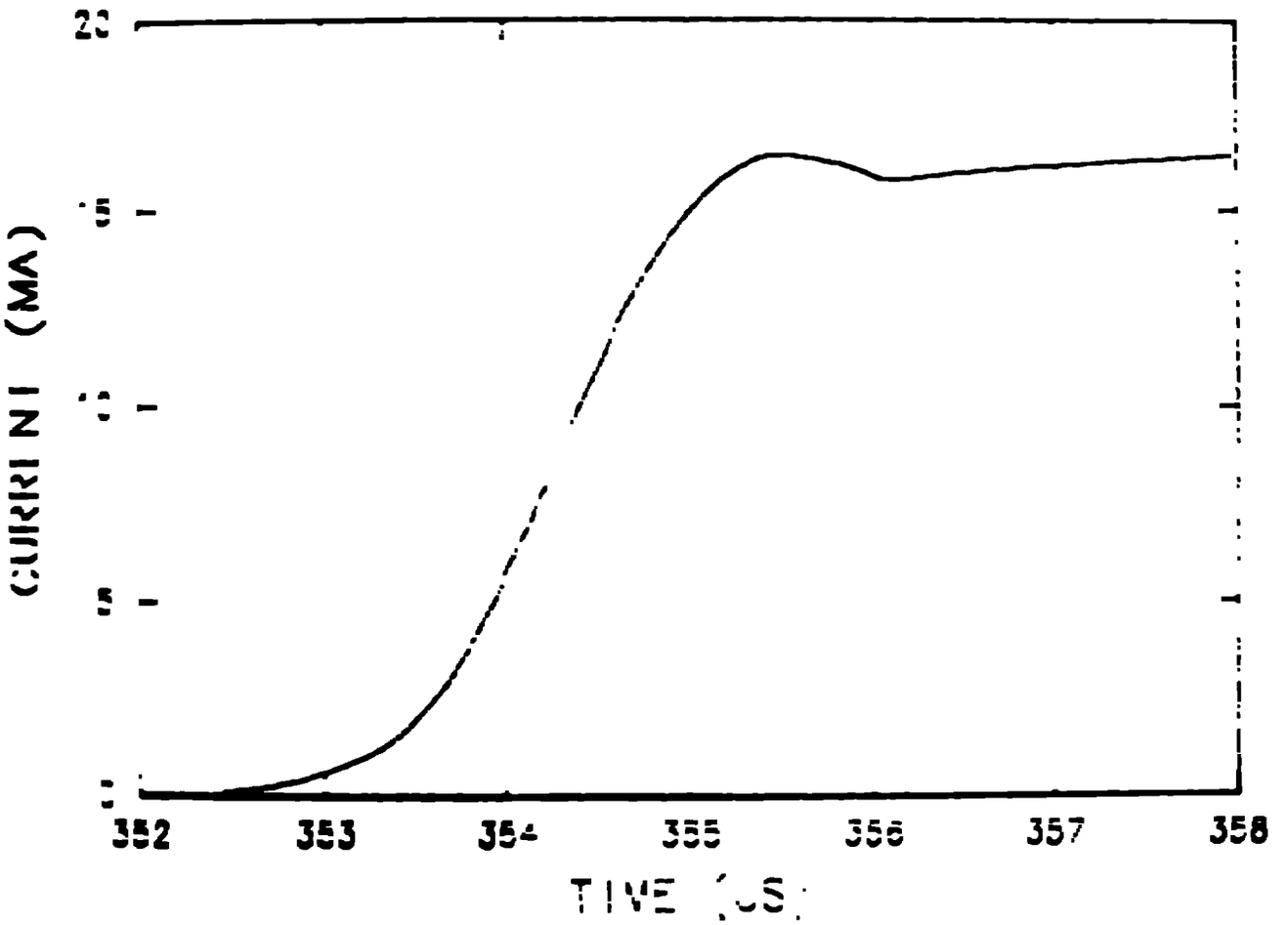

Fig. 13 PFS current profile taken off typical Faraday rotation signal Peak is 16.4 MA and 11 - 89% risetime is 1.56 us

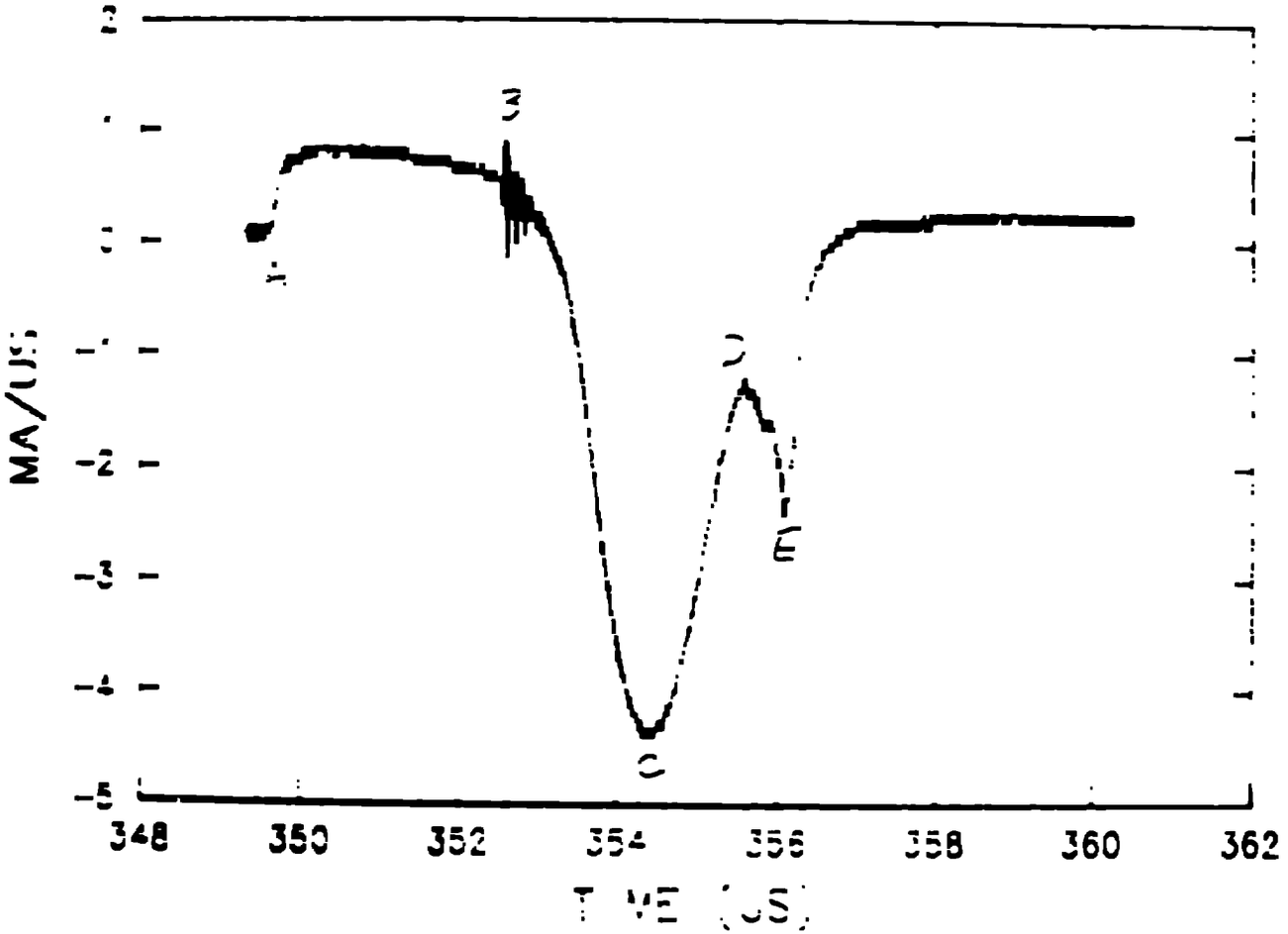

Fig. 14 dI_{sto}/dt with positions of various events marked. A- first motion of EFF conductor B- closing of detonator actuated switches C- Peak transfer rate to PFS. D- Onset of flux transfer into load slot E. Peak transfer rate into load slot.

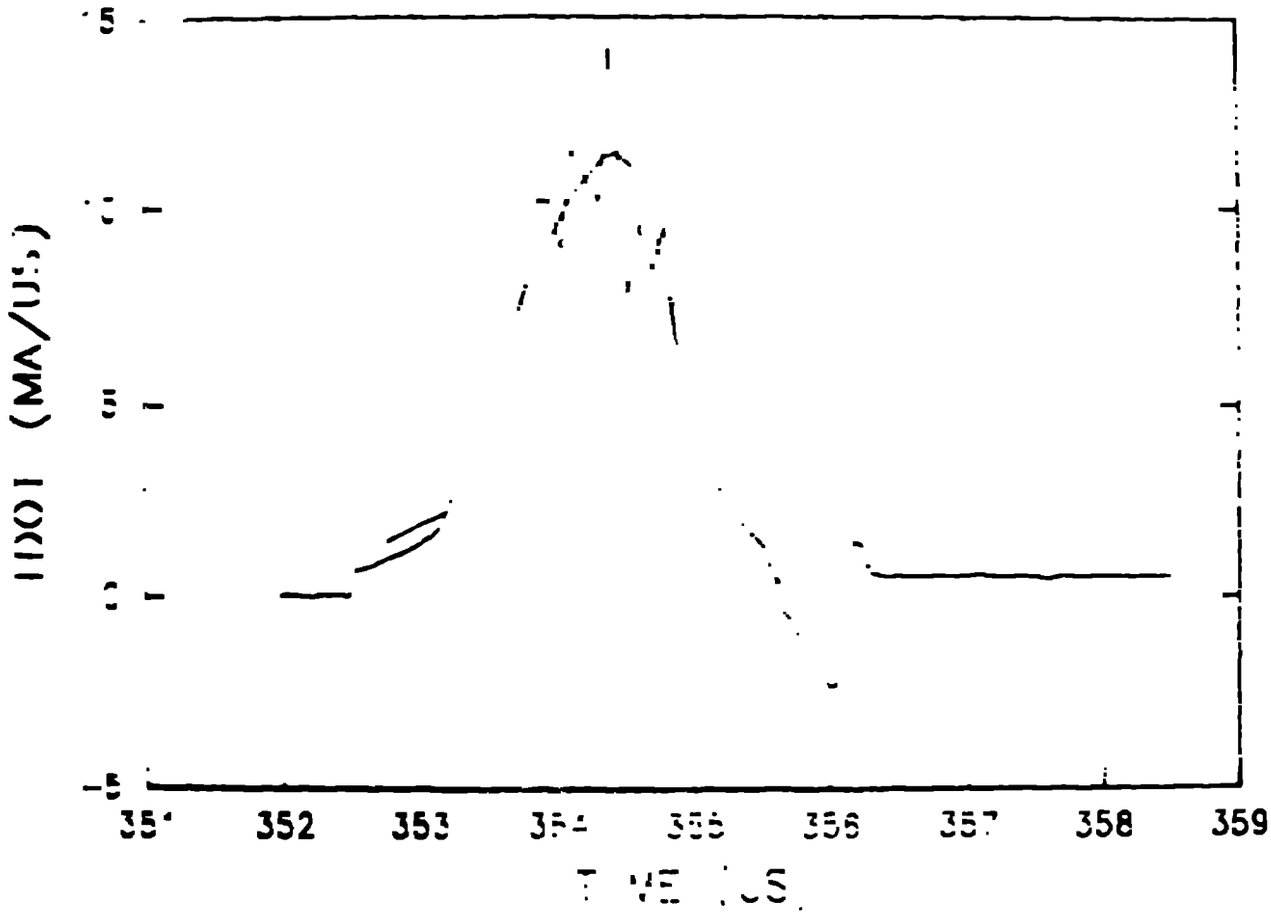

Fig. 15 $d(I_{PFS})/dt$ combined from Rogowski coil and Faraday rotation sensors. A crude smoothing is drawn through the jagged peak area, and we estimate a peak of 11.5 MA/μs.

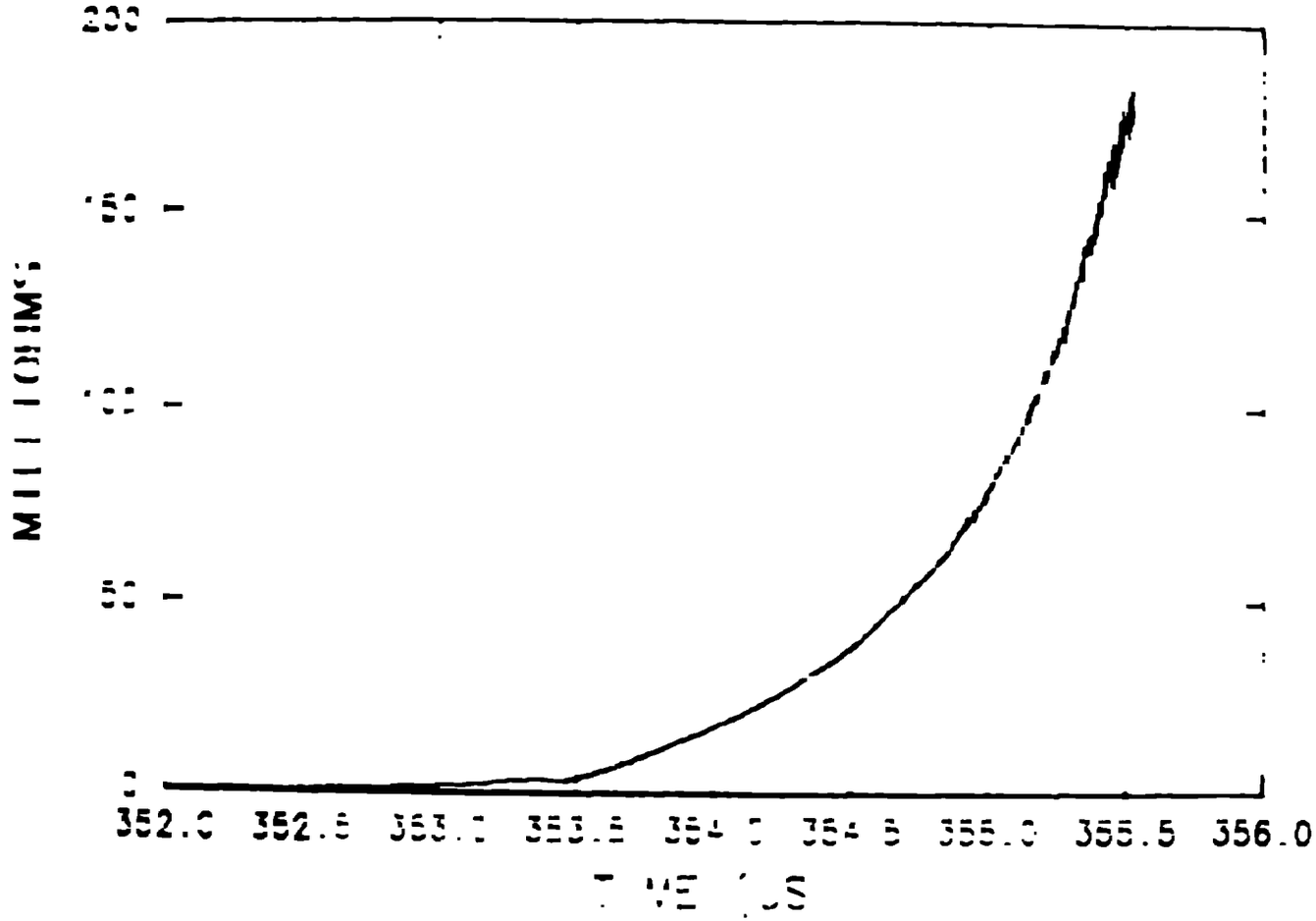

Fig 1: Resistance in the EFF as determined from experimental data. Points prior to 353.4 come from T2, with values synchronized to T3 by resistance determined from the initial dip, ΔT step and I_{STO}. The T2 points came directly from voltage and current measurements.

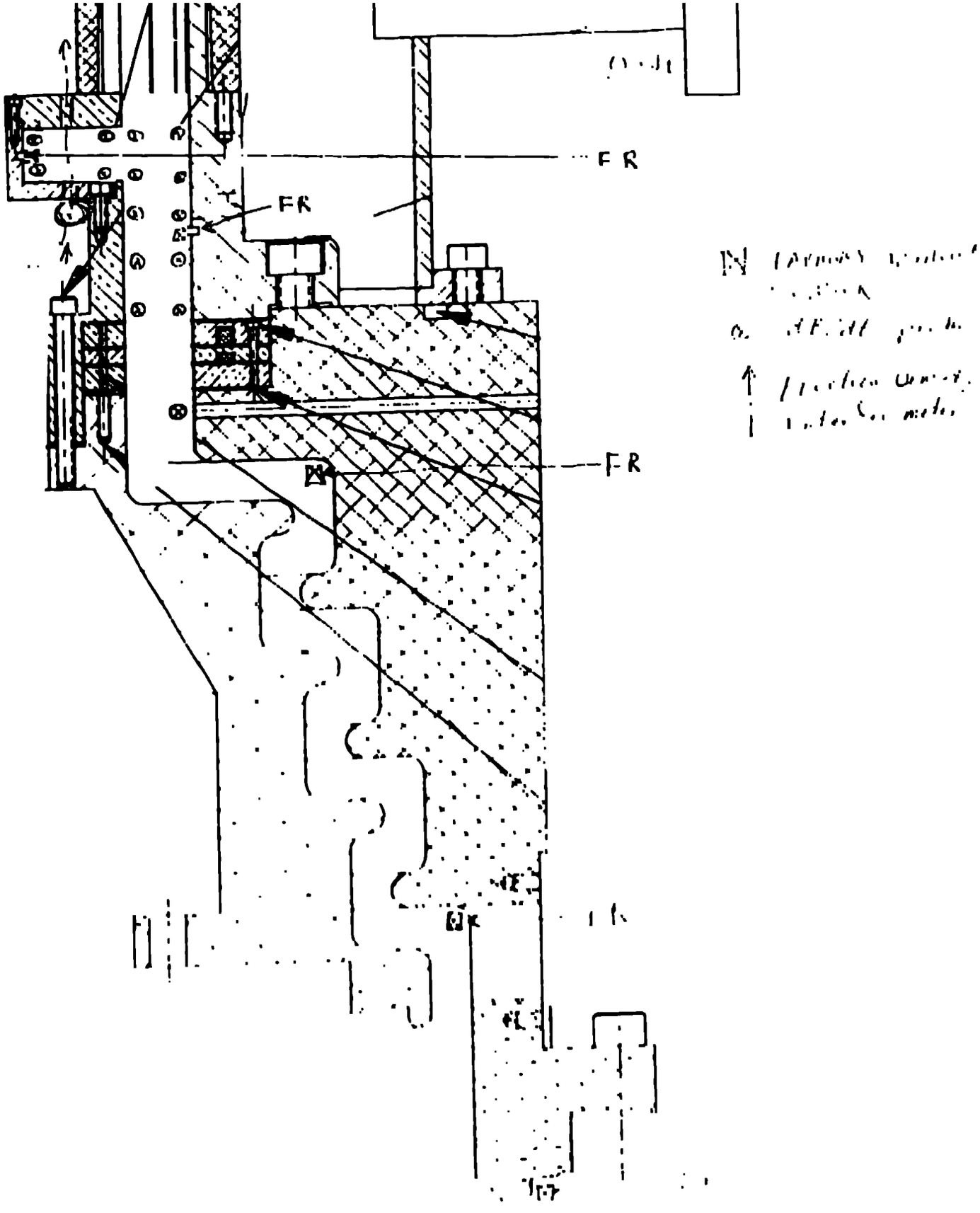

Fig. 17 Probe locations for array of 36 dB/dt probes and 8 Faraday rotation sensors in the 14 load. Most dB/dt probes were in groups of two, 180 degrees apart. No two probes were immediately across the channel from each other, but were at different azimuthal

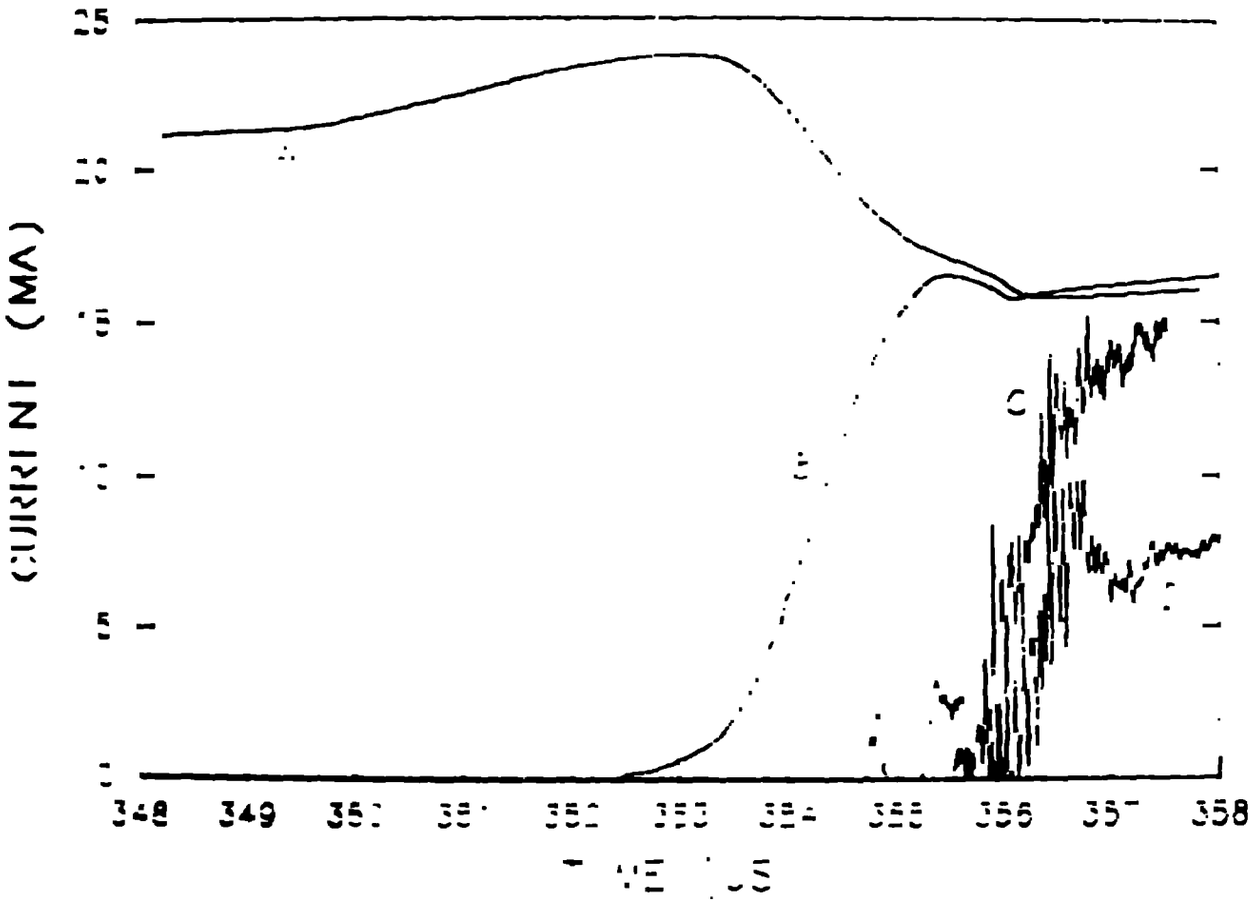

Fig. 18 Selected current signals from T3. A- Storage inductor current. B- Typical Faraday sensor signal showing PFS current. C- dB/dt sensor (integrated) 5.8 cm from graded foil on inside electrode. D- dB/dt sensor (integrated) 5.8 cm from graded foil on

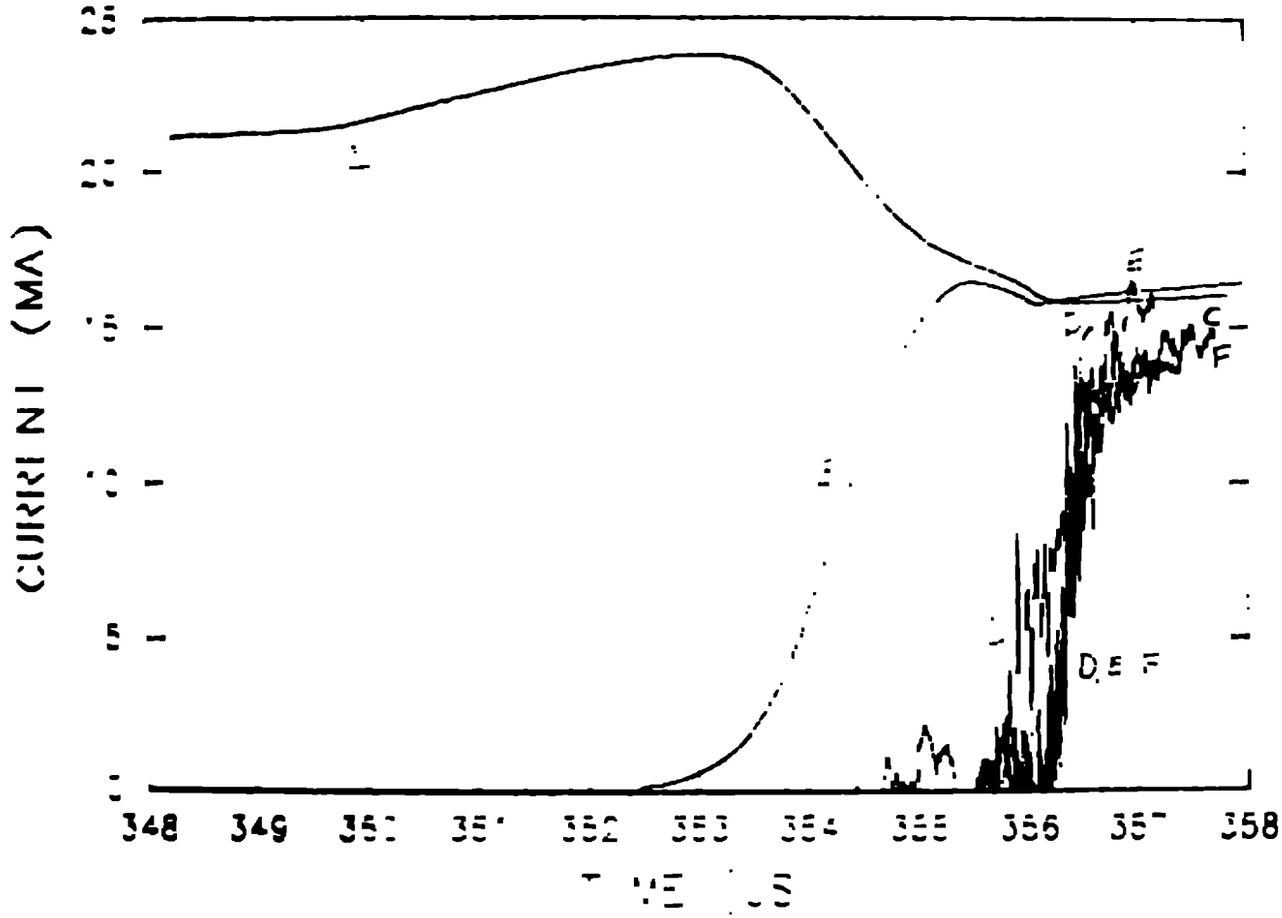

Fig. 14 Selected current signals from T3. A- Storage inductor current B- Typical Faraday sensor signal showing PFS current C- dB dt sensor (integrated) 5.8 cm from graded foil on inside electrode D- Most optimistic interpretation of Faraday sensor in load slot bottom E- dB dt sensor (integrated) recessed inside load slot on upstream side. F- dB dt sensor (integrated) in bottom of load slot.

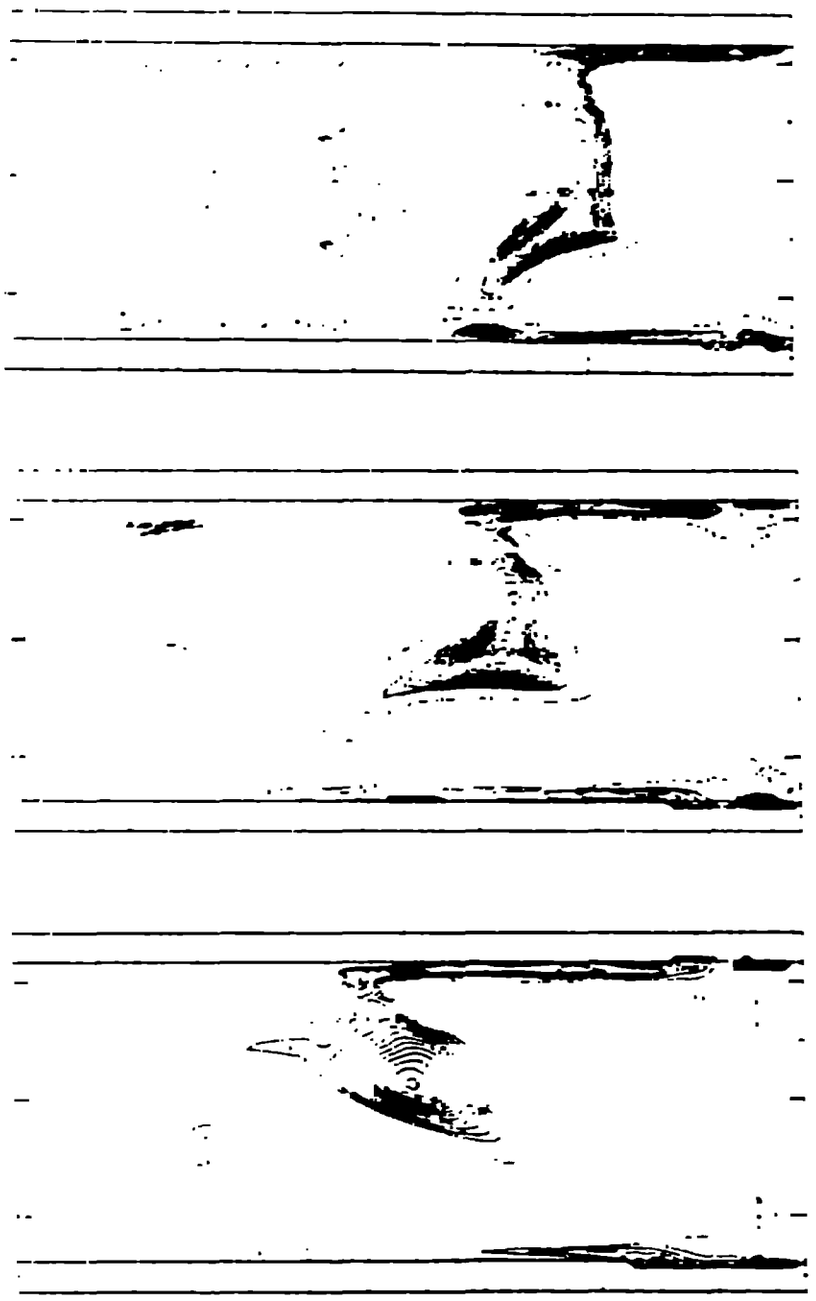

Fig. 20 2D RMHD calculations of a 1 r gun plasma driven with T3 waveform Frame 1, at 3 3μs, shows onset of mass-thinning. Frame 2, at 3.5μs, shows that flux has flooded through the gun plasma Frame 3, at 3 7μs, shows that the PFS has opened and remains so